

Direct Extraction of Tumor Response Based on Ensemble Empirical Mode Decomposition for Image Reconstruction of Early Breast Cancer Detection by UWB

Qinwei Li, Xia Xiao, *Member, IEEE*, Liang Wang, Hang Song, Hayato Kono, Peifang Liu, Hong Lu, and Takamaro Kikkawa, *Fellow, IEEE*

Abstract—A direct extraction method of tumor response based on ensemble empirical mode decomposition (EEMD) is proposed for early breast cancer detection by ultra-wide band (UWB) microwave imaging. With this approach, the image reconstruction for the tumor detection can be realized with only extracted signals from as-detected waveforms. The calibration process executed in the previous research for obtaining reference waveforms which stand for signals detected from the tumor-free model is not required. The correctness of the method is testified by successfully detecting a 4 mm tumor located inside the glandular region in one breast model and by the model located at the interface between the gland and the fat, respectively. The reliability of the method is checked by distinguishing a tumor buried in the glandular tissue whose dielectric constant is 35. The feasibility of the method is confirmed by showing the correct tumor information in both simulation results and experimental results for the realistic 3-D printed breast phantom.

Index Terms—Breast cancer detection, ensemble empirical mode decomposition (EEMD), tumor response extraction, ultra-wide band (UWB).

I. INTRODUCTION

BREAST cancer has been one of the most common diseases which cause many women's death throughout the world. The early breast cancer detection is detecting the tumor when it is at early stage, which could help heal the patients and would not harm the women's health. It is clear that the best way to control this disease is detecting it at an early stage [1]. Early

detection can urge patients to get prompt treatment and thus will help improve the survival rates. Early breast cancer detection has been proved to help patients to obtain prompt treatment and increase their life expectancy through efforts. Currently, X-ray mammography is the conventional technique utilized for the breast cancer detection [2], [3]. However, the sensitivity is reduced in dense breast tissue, and the exposure to ionizing radiation will limit the use of this screening technique [4]. Other methods such as the Magnetic Resonance Image (MRI) might detect this early breast cancer detection. However, there are some fatal flaws such as the high expenses and often inaccessible for large volume of patients. And when the diameter of the tumor is smaller than the distance of the MRI detecting slices, the MRI detection will miss the target. Approximately 4%-34% of all breast cancers are missed by conventional mammography [5], [6]. Therefore, these methods cannot be used frequently. The breast cancer detection needs to be taken frequently, only in this way can the women's health be protected. So there is tremendous amount of research in harmless imaging methods with high resolution. In recent years, various microwave imaging techniques have been used in early breast cancer detection, such as ultra-wide band (UWB) microwave imaging technique, microwave tomography and so on. UWB microwave imaging method is a radiationless, low-cost and high-resolution technique which has attracted considerable attention in recent years [7]. This technique is based on the big contrast of the dielectric properties between normal breast tissues and the malignant breast tissue [8]. However, the problem is the big clutters from normal tissues and the strong backscatter from the breast skin, in which the signal from the tumor is embedded. Currently, one of the most common methods of removing these clutters is using the tumor-free model, from which the detected signal is used as the calibration waveform [9], [10]. Then the tumor response can be obtained by subtracting the calibration waveform from signals detected from the tumor-contained breast model. However, in clinical cases, the tumor-free model cannot be obtained easily as different people has different breast configuration. Even the ideal tumor-free model is constructed for each detection, there would be distinctions between the real breast and the ideal tumor-free model, which may bring errors and make the procedure of detection much more complicated.

Manuscript received January 14, 2015; revised May 28, 2015; accepted August 31, 2015. Date of publication November 03, 2015; date of current version November 24, 2015. This work was supported by the National Natural Science Foundation of China (Grant 61271323) and in part by the Japan Science and Technology agency (Advanced Measurement and Analysis). This paper was recommended by Associate Editor W.-C. Fang. (*Corresponding Author: X. Xiao.*)

Q. Li, X. Xiao, L. Wang, and H. Song are with the School of Electronic and Information Engineering, Tianjin University, Tianjin 300072, China (e-mail: xiaoxiao@tju.edu.cn).

H. Kono and T. Kikkawa are with the Research Institute for Nanodevice and Bio Systems, Hiroshima University, Higashi-Hiroshima 739-8527, Japan.

P. Liu and H. Lu are with the Department of Breast Imaging, Tianjin Medical University Cancer Institute and Hospital, Key Laboratory of Breast Cancer Prevention and Therapy, Ministry of Education of China, Tianjin 300060, China.

Color versions of one or more of the figures in this paper are available online at <http://ieeexplore.ieee.org>.

Digital Object Identifier 10.1109/TBCAS.2015.2481940

The aim of this paper is to overcome the aforementioned problem by proposing a novel signal processing approach, which could extract the tumor response directly from the as-detected signals obtained from the tumor-contained breast model. The proposed method could obtain the tumor signal directly from received signals without the employment of the tumor-free model or any other calibration waveforms. Therefore, a data-dependent adaptive method is needed. Empirical mode decomposition (EMD) approach provides a facility to help meet the requirement which is mentioned before. The EMD is an adaptive time-frequency signal processing approach that has better effect in analyzing nonstationary and nonlinear data [11]. The EMD has been successfully utilized in machinery fault diagnosis and structural damage detection [12], [13]. The EMD method can decompose any complex signal into a collection of adaptive components, called intrinsic mode functions (IMFs) [14]. However, the IMFs obtained by using this method have mixed components, which fail to perform an accurate estimation of the tumor signal extraction. Considering the mode mixing problem, a noise assisted data analysis method called ensemble empirical mode decomposition (EEMD), which is introduced by Wu and Huang [15], [16], is applied in decomposing the received signals to extract the tumor response in this study.

This paper proposes a tumor signal extraction method based on EEMD approach, and verifies its effectiveness in two different models that are introduced in Section II. The Section III gives the detail of the signal processing procedure applied for directly extracting the tumor responses. Section IV presents the reconstructed images resulted from the proposed method as well as the images from the previous process with the need of the calibration waveforms. Finally a conclusion to this paper is given in Section V.

II. SYSTEM CONFIGURATION

A. MRI-Derived Breast Model

In many early studies, the models that are used in computational simulation are relative ideal. In those phantoms, the specific tissues and the whole breast are combined with classical geometry shapes. However, the early breast cancer detection technique needs to approach the real situation. More realistic models in terms of the tissues, shape and so on are needed for UWB breast cancer detection technique. Therefore, the higher accuracy models used for the electromagnetic analysis are created based on the Magnetic Resonance Image (MRI) shown in Figs. 1 and 3. These two MRIs are from two different types of breast of two patients. They are used in this study to verify the effectiveness of the proposed method.

These two phantoms are derived from the MRIs of the patients. As shown in Figs. 1 and 3, the fat, glandular tissues and the chest wall can be identified by using the gray value. All MRIs are transformed from Digital Imaging and Communications in Medicine (DICOM) files and normalized into unit 8 gray-scale range. Then the image is read as gray-value pictures and resized to 640×640 pixels. In this resolution, one pixel is exactly represented $0.5 \text{ mm} \times 0.5 \text{ mm}$ square of the real breast. The pixels ranged from 1 to 70 and 570 to 640, are cut

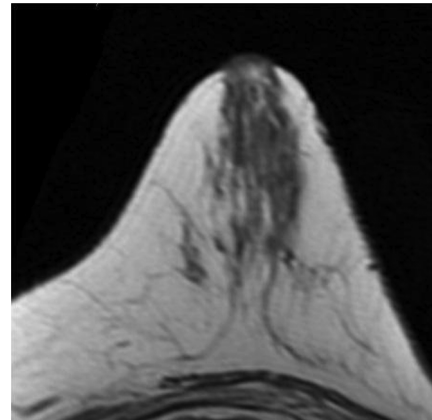


Fig. 1. A magnetic resonance image (MRI) of a breast I.

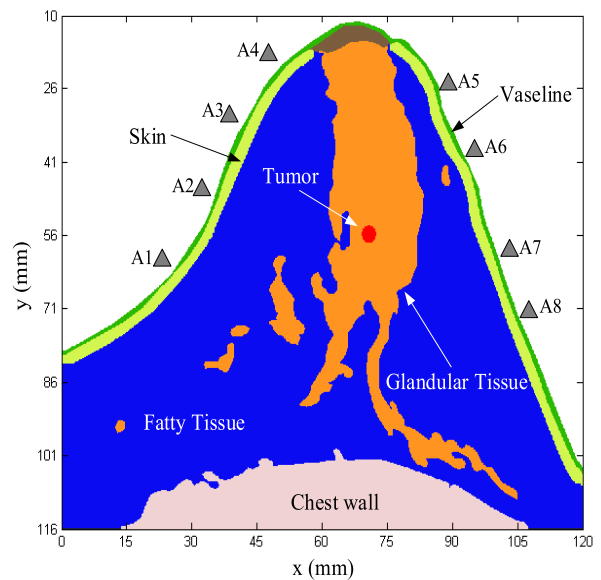


Fig. 2. Geometry configuration I of the breast numerical phantom derived from the Magnetic Resonance Image scan shown in Fig. 1.

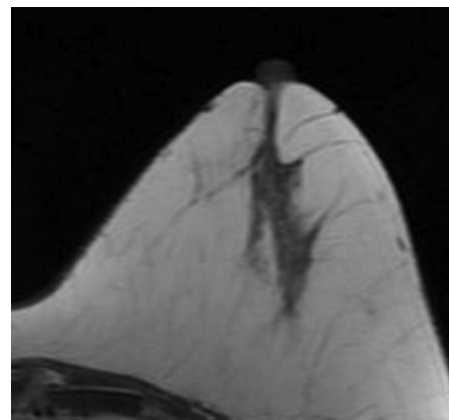


Fig. 3. A magnetic resonance image (MRI) of a breast II.

in order to remove the unclear margin of the MRI. Then the Canny edge detection algorithm is applied to find the boundary between the fatty tissues and air. Then all the tissues in the breast

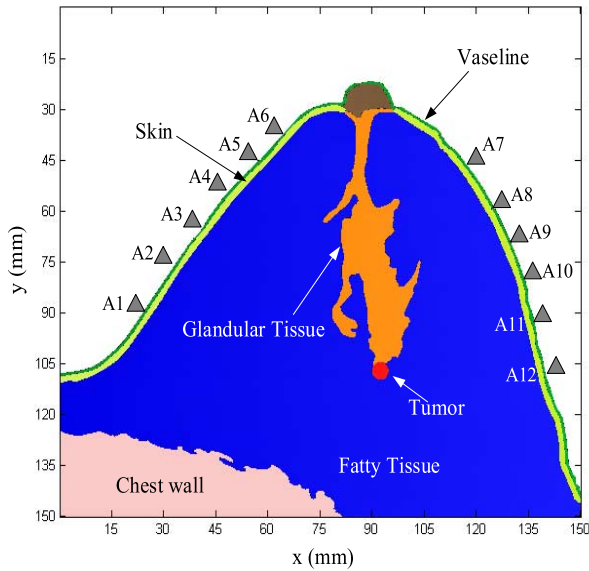


Fig. 4. Geometry configuration II of the breast numerical phantom derived from the Magnetic Resonance Image scan shown in Fig. 3.

can be extracted and mapped into corresponding dielectric properties [17], [18]. Fig. 2 shows the derived model I, whose size is 120 mm \times 116 mm. The breast tissues such as the skin, glandular tissue, chest wall, and the fatty tissue are all contained in this model. The assumed tumor with a diameter of 4 mm is embedded inside the glandular tissue for this research, and its specific place is $x = 71$ mm, $y = 57$ mm. The skin layer is placed around the breast phantom and has varying thickness changing between 2 mm and 3 mm. The outermost layer which is just around the skin layer is matching medium Vaseline. This matching medium with a dielectric constant of 2.2 is employed onto the skin to improve the performance of the antenna [19]. Fig. 4 shows the model II that is derived from the MRI shown in Fig. 3. And the size of this second model is 150 mm \times 150 mm. This phantom also contains all the breast tissues such as the skin, glandular tissue, chest wall, and the fatty tissue, but the model II is very different from the model I to check the feasibility of the proposed method. Besides, to investigate the influence of the clutter interference during the tumor detection, a tumor with a diameter of 4 mm is assumed to be embedded at the bottom and the interface of the glandular tissue, which is a more complicate situation. This tumor is located at the place of $x = 95$ mm, $y = 105$ mm. The parameters of the skin layer and the Vaseline around the model II is just the same as model I.

B. Antenna Arrangement and Simulation Process

As shown in Fig. 2, an eight-element antenna array A1- A8 is arranged around the surface of the model I. And the Fig. 4 shows an antenna array composed of twelve antennas A1-A12 is placed around the surface of model II, whose size is bigger than model I. The antenna design is a very important part of the system configuration. As the sufficient information needs to be collected for good image quality, the antennas should be able to

TABLE I
ELECTRIC PROPERTIES OF THE TISSUES IN MODEL I [20]

| | Fatty tissue | Chest wall | Glandular tissue | Tumor | Skin |
|----------------|--------------|------------|------------------|-------|------|
| ϵ_r | 9.8 | 50.8 | 14 | 50 | 34.7 |
| σ (S/m) | 0.4 | 7 | 0.5 | 4.8 | 3.9 |

TABLE II
ELECTRIC PROPERTIES OF THE TISSUES IN MODEL II [21], [22]

| | Fatty tissue | Chest wall | Glandular tissue | Tumor | Skin |
|----------------|--------------|------------|------------------|-------|------|
| ϵ_r | 10 | 50 | 35 | 50 | 34.7 |
| σ (S/m) | 0.4 | 7 | 0.5 | 4.8 | 3.9 |

operate over a wide band of frequencies. The antenna should be small so that enough antennas can be arranged around the surface of the breast. In these two models, a slot on-body antenna whose detail design is reported in [20] has been employed as a good candidate. During this detection, a Gaussian monocycle pulse with a center frequency of 6 GHz is emitted from one antenna alternately and the backscattered signals are received by the rest of antennas. Then repeat this step for all the antennas to get the whole series of signals.

Both the electromagnetic properties and spatial heterogeneity of all the breast tissues are considered in the two models. The dielectric constant ϵ_r and the conductivity σ of each tissue in model I referred from [21] are shown in Table I. In addition, the contrast of dielectric constant between the tumor and the glandular tissue, which is smaller than it is in the previous research case, is used to investigate the feasibility of this method. The dielectric constant of the glandular tissue in model II is much larger than it is in model I. In this way, the dielectric constant contrast between the glandular tissue and the tumor will be less significant. So the clutter from the glandular tissue will be stronger than before. In this situation, the extraction of the tumor response is much more difficult than before. The dielectric constant ϵ_r and the conductivity σ of each tissue in model II are shown in Table II [22], [23].

III. SIGNAL PROCESSING

In this section, the detail of the proposed signal processing technique in this paper is described. The principle of the ensemble empirical mode decomposition (EEMD) has been reviewed in this section. Then the selection of the optimal parameters that are applied in this approach and the extraction of tumor response signals will be described in detail. Also, in this section, model I is used as the example.

A. Principle of Ensemble Empirical Mode Decomposition

Empirical mode decomposition (EMD) is a method that is often considered to analyze the nonlinear and nonstationary signals. It can be applied to decompose the signals into a series of intrinsic mode functions (IMFs). The IMFs have two following conditions [24]:

- 1) The number of extrema (the sum of the number of maxima and minima) and the number of the zero crossings should be equal or at most differ by one.
- 2) The mean of the envelope defined by local maxima and the envelope defined by local minima should be zero.

With the above definition of the IMFs, the given signal $x(t)$ can be decomposed by the following steps [25]:

- 1) Identify all the local maxima and the local minima of the signal $x(t)$. Then apply the cubic spline function to interpolate the local maxima and the local minima so that the upper envelope $e_{\max}(t)$ and the lower envelope $e_{\min}(t)$ can be obtained.
- 2) Calculate the mean of the upper envelope and the lower envelope $m_1(t)$ by

$$m_1(t) = \frac{\{e_{\max}(t) + e_{\min}(t)\}}{2}. \quad (1)$$

- 3) Compute the difference between the original signal $x(t)$ and the mean $m_1(t)$, then the first component $h_1(t)$ can be obtained as

$$h_1(t) = x(t) - m_1(t). \quad (2)$$

- 4) Treat $h_1(t)$ as the next original signal in the next iteration, and repeat the above steps until the first IMF $c_1(t)$ is obtained. Then separate $c_1(t)$ from the original signal $x(t)$ to get the residue $r_1(t)$ by

$$r_1(t) = x(t) - c_1(t). \quad (3)$$

- 5) Replace the signal $x(t)$ with $r_1(t)$, then repeat the first step to the fourth step until all the IMFs are obtained. Finally the signal $x(t)$ could thus expressed as

$$x(t) = \sum_{n=1}^N c_n(t) + r_N(t) \quad (4)$$

where $c_n(t)$ means the n^{th} IMF, $r_N(t)$ represents the trend, which is a monotonic function with no more than two extremes.

However, the EMD algorithm has its own shortcoming of the mode mixing, which is defined as a single IMF including oscillations of dramatically disparate scales, or the component of a similar scale residing in different IMFs. This shortcoming always influences the accuracy of the results. To overcome this intrinsic problem, the ensemble empirical mode decomposition (EEMD) is introduced by [26] to improve the decomposition capability of the algorithm. The EEMD method is developed from the EMD method. It is a noise assisted signal analysis method and has been proven to be with better scale separation ability than the EMD method. The procedure of the EEMD method can be briefly summarized as follows:

- 1) Add a white noise $n(t)$ to the original signal. Then the new signal $y(t)$ can be represented by

$$y(t) = x(t) + \beta n(t) \quad (5)$$

where β is the magnitude of the added white noise.

- 2) Decompose the new signal $y(t)$ by using EMD method into a series of IMFs.
- 3) Repeat the above steps M times by applying different white noise with different magnitude each time. In this way, all the IMFs will be obtained.
- 4) Calculate the ensemble means of all the IMFs, then the final results will be obtained by

$$c_i(t) = \frac{1}{M} \sum_{m=1}^M c_i^m(t). \quad (6)$$

Based on the property of zero mean of the white noise, the effects that are caused by the white noise can be cancelled out in the final ensemble mean if there are sufficient trials. In this way, the EEMD can effectively resolve the problem of mode mixing, which is caused by EMD.

B. Parameter Selection

In EEMD algorithm, two critical parameters, the magnitude of the white noise β and the ensemble number M , need to be selected for different trials. The amplitude of the added white noise should be chosen appropriately for good performance of the EEMD method. The added white noise will not be cancelled out after the ensemble process if the amplitude of the added white noise is too large. Meanwhile, the problem of mode mixing may still exist if the amplitude of the white noise is too small. Once the amplitude of the white noise is determined, increasing the ensemble number is very helpful for EEMD to reduce the remaining noise in each IMF. However, to some degree, continuing increasing the ensemble number results in only a minor change in errors. The larger the ensemble number is, the more time will be taken for the computation. In the previous research, the selection of these two parameters needs to satisfy the condition described by Wu and Huang with

$$\ln e + \frac{\beta}{2} \times \ln M = 0 \quad (7)$$

where the parameter e represents the standard deviation of error between the original signal and the corresponding IMF. The amplitude of the white noise can be expressed as

$$\beta = L \times \sigma_0 \quad (8)$$

where the parameter σ_0 is the standard deviation of the original signal and L is the noise level of the added white noise.

However, by following the rule shown in (7), the amplitude of the white noise should be set as about 0.3 of the standard deviation of the original signal and the value of ensemble number is over a few hundred [27], which are empirical numbers. The rule shown in (7) is not always usable for signal processing in

different applications. In this experiment, new method is applied to set the parameters.

The relative root mean square error (RMSE) can be introduced to evaluate the performance of EEMD by trying different levels of the added white noise [28]. In this way, the optimal level of the white noise can be determined by applying the relative RMSE by

$$\text{Relative RMSE} = \sqrt{\frac{\sum_{k=1}^N (x(k) - c_{\max}(k))^2}{\sum_{k=1}^N x^2(k)}} \quad (9)$$

where the $x(k)$ represents the original signal, $c_{\max}(k)$ represents the IMF which has the highest correlation with the original signal. The parameter N is the number of the samples in the original signal. The desired decomposition will separate the main signal component from noise and other low-correlated signal components. There must be a value of noise amplitude that maximizes the relative RMSE. If the relative RMSE is very small and close to zero, it indicates that the selected IMF, $c_{\max}(k)$, is close to the original signal, that is to say, the selected IMF, $c_{\max}(k)$, contains not only the main component in the original signal but also part of noise and the other low-correlated or irrelevant signal components. Accordingly, the difference between the original signal and the selected IMF is small and the desired decomposition is not reached. At this point, the selected IMF, $c_{\max}(k)$, only contains the main signal component, and is separated from noise and the other irrelevant signal components. The error is from the remaining components in the original signal, other than the selected IMF. This is the desired decomposition result and the corresponding noise amplitude is the optimal one. The procedure of determining the optimal noise level is as follows.

First, set a small value of the ensemble number, and an initial noise level. Second, perform the EEMD to decompose the original signal and calculate the relative RMSE. Only the IMF with the highest correlation coefficient related to the original signal is needed to calculate the relative RMSE. Third, increase the noise level, and repeat the step two. The most appropriate noise level is the value that maximizes the relative RMSE. In this way, the level of the white noise can be determined.

After determining the noise level, the value of the ensemble number should be chosen for decomposing the all the received signals. The setting of added white noise and the selection of M are two separate parts in this experiment. The effects of the decomposition using the EEMD are that the added white noise series cancel each other in the final mean of the corresponding IMFs. No matter what the setting of the added white noise is, the M should be large enough to eliminate the added white noise at the end of the trial. If the ensemble number is too small, the white noise remained in each IMF will not be cancelled out. So a larger value of ensemble number will lead to a smaller error, which is mainly caused by the added white noise, especially for the high-frequency component. However, a large ensemble number will lead a large computation cost. So if there is very

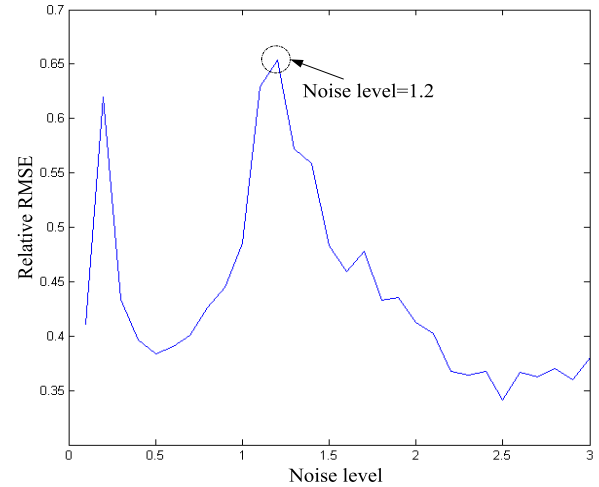


Fig. 5. The value of relative RMSE with different noise level in model I.

small change in the errors, the ensemble number can be determined.

C. Tumor Response Extraction

The EEMD method is applied in our research for the early breast cancer detection. During the detection procedure, a Gaussian monocycle pulse with a center frequency of 6 GHz is emitted from one antenna alternately and the backscattered signals are received by all the other antennas. Then repeat this step for all the antennas to get the whole series of signals. All the collected signals will be decomposed by the optimal EEMD algorithm. The model I shown in Fig. 2 is used to explain the processing procedure of the optimal EEMD method during the breast cancer detection in detail in this part.

As shown in Fig. 5, during this trial, when the noise level is 1.2, the value of the relative RMSE is the largest. As is mentioned before, the larger the ensemble number, the more time will be taken for the computation. When the value of the ensemble number is over 50, there is almost no change in errors. So the ensemble number 50 is used as the ensemble number in our research for breast cancer detection. Better decomposition performance can be obtained by setting the optimal noise level for these all signals as 1.2 and the ensemble number M as 50. For instance, Fig. 6 shows the detected signal in the case of the impulse emitted from the antenna A1 and received by the antenna A3 and the decomposing results of this signal by using EEMD algorithm. The signal has been decomposed into 13 IMFs (C1 to C13) and a residue (r13). To investigate the regulation of the EEMD method in this application, Figs. 7 and 8 are presented for the detection cases in which the emitter and the detector are located at the different sides of the breast model. In Fig. 7, the impulse is emitted from antenna A3 and received by antenna A7, these two antennas are located at different sides of the breast model. In Fig. 8, the impulse is emitted from antenna A5 and received by antenna A8, this signal represents the collected signals of the right side of the antennas. The tumor response signal can be extracted from these IMFs through the further signal processing.

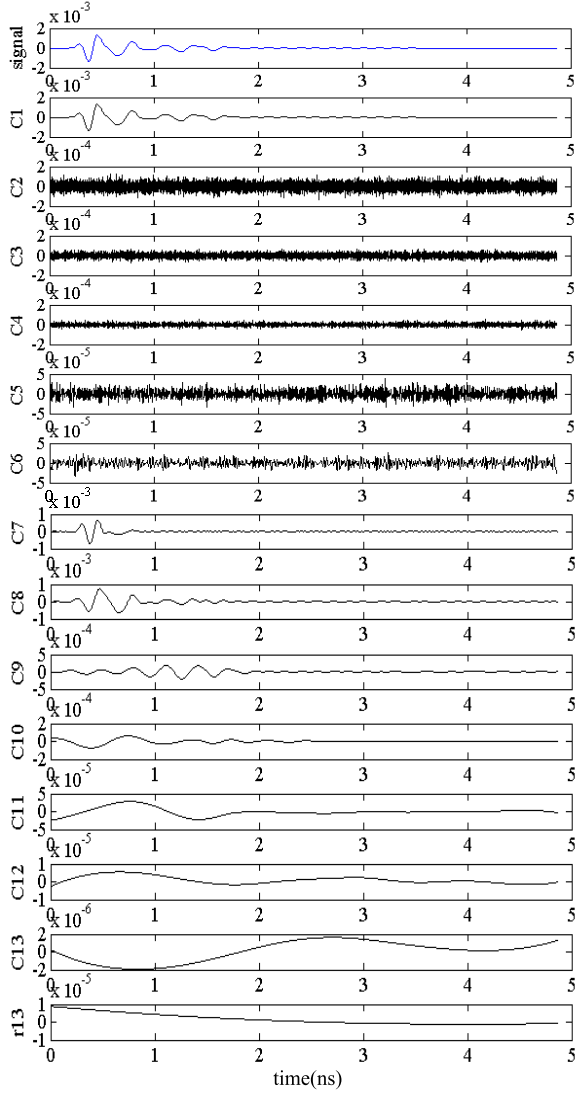


Fig. 6. IMFs (C1 to C13) of the detected signal in the case of the impulse emitted from antenna A1 and received from antenna A3 in model I. The r13 is the residual of the signal after the EEMD processing.

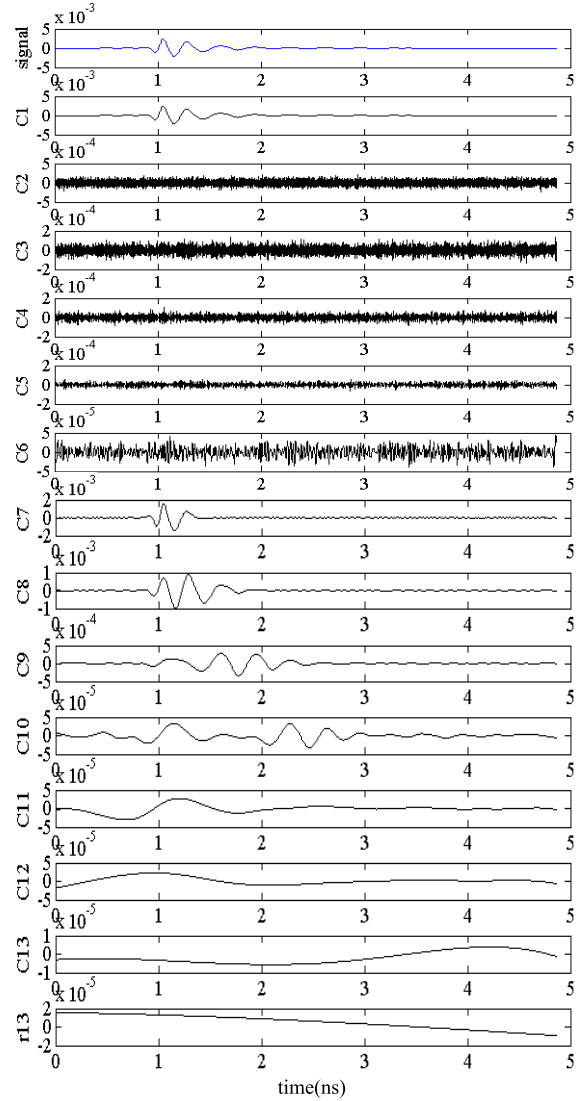


Fig. 7. IMFs (C1 to C13) of the detected signal in the case of the impulse emitted from antenna A3 and received from antenna A7 in model I. The r13 is the residual of the signal after the EEMD processing.

The Pearson’s Correlation Coefficient [30], [31] x_g , is widely used in statistical analysis and pattern recognition. To extract the tumor response from all the IMFs that are obtained by the optimal EEMD method, the Pearson’s correlation coefficient has been used in this section. The Pearson’s correlation coefficient is described by

$$x_g = \frac{\sum_{k=1}^N (x(k) - \overline{x(k)}) (c_n(k) - \overline{c_n(k)})}{\sqrt{\sum_{k=1}^N (x(k) - \overline{x(k)})^2} \sqrt{\sum_{k=1}^N (c_n(k) - \overline{c_n(k)})^2}} \quad (10)$$

where the parameter N is the number of the samples in the original signal, $x(k)$ is the original signal, $\overline{x(k)}$ is the mean of the original signal, $c_n(k)$ is the n^{th} IMF, and $\overline{c_n(k)}$ is the mean of the n^{th} IMF. If the correlation coefficient is close to 1, it means this IMF correlates the original signal. If the correlation coefficient is close to 0, it means the IMF is uncorrelated with the

original signal. Table III shows the correlation coefficients of all the IMFs obtained from the as-detected signal, which is in the case of the impulse emitted from the antenna A1 and received by the antenna A3. Table IV shows the correlation coefficients of all the IMFs achieved from the as-detected signal, which is in the case of the impulse emitted from the antenna A3 and received by the antenna A7. Table V shows the correlation coefficients of all the IMFs obtained from the as-detected signal, which is in the case of the impulse emitted from the antenna A5 and received by the antenna A8. As shown in these three tables, the correlation coefficient of the first IMF (C1) is equal to 1, because the first IMF (C1) is just the as-detected signal itself. The correlation coefficients of 7th IMF (C7) and 8th IMF (C8) are much bigger than the others. So it can be identified that the 7th IMF (C7) and 8th IMF (C8) contain most of the tumor information [29].

The correlation coefficients of all the IMFs can evaluate the possible relative main component of the signal. But using the

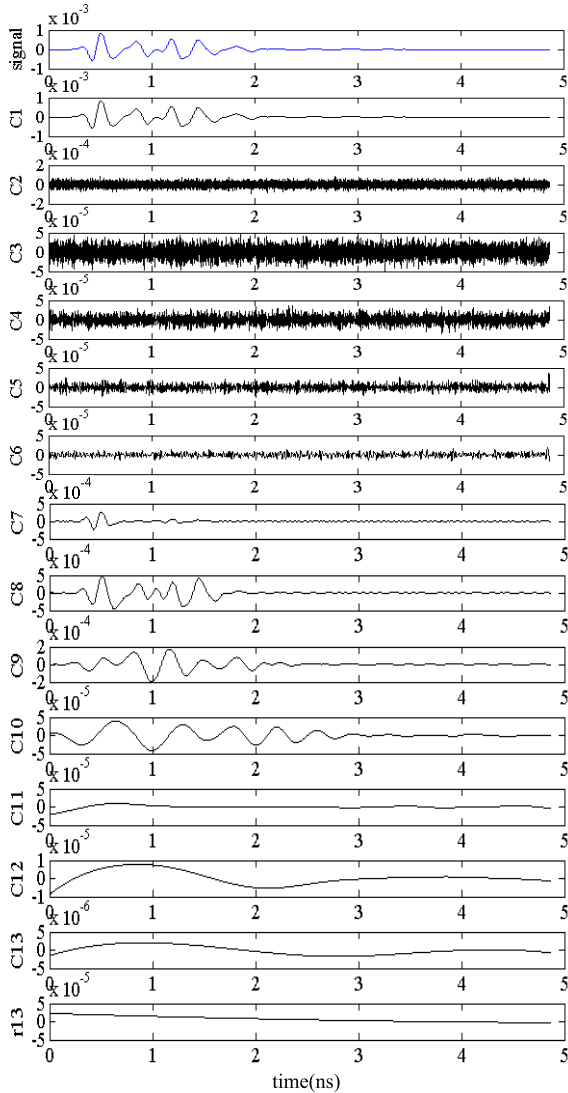


Fig. 8. IMFs (C1 to C13) of the detected signal in the case of the impulse emitted from antenna A5 and received from antenna A8 in model I. The r13 is the residual of the signal after the EEMD processing.

TABLE III

THE CORRELATION COEFFICIENTS BETWEEN THE DETECTED SIGNAL AND ALL THE IMF'S RESPECTIVELY (THE SIGNAL IS IN THE CASE OF THE IMPULSE EMITTED FROM ANTENNA A1 AND RECEIVED BY ANTENNA A3) IN MODEL I

| IMFs | C1 | C2 | C3 | C4 | C5 | C6 | C7 |
|-------------------------|-------|-------|--------|-------|-------|-------|-------|
| Correlation coefficient | 1 | 0.005 | 0.002 | 0.004 | 0.015 | 0.025 | 0.772 |
| IMFs | C8 | C9 | C10 | C11 | C12 | C13 | r13 |
| Correlation coefficient | 0.923 | 0.583 | -0.003 | -4e-4 | -2e-4 | 9e-6 | 2e-5 |

correlation coefficients to extract the tumor information will not lead to good results. So the kurtosis value can be introduced to distinguish the tumor information and the relevant extraction results.

To eliminate more clutters and extract the tumor response, further study is carried out to find the most correlated IMF corresponding to the tumor information. In this way, the kurtosis

TABLE IV

THE CORRELATION COEFFICIENTS BETWEEN THE DETECTED SIGNAL AND ALL THE IMF'S RESPECTIVELY (THE SIGNAL IS IN THE CASE OF THE IMPULSE EMITTED FROM ANTENNA A3 AND RECEIVED BY ANTENNA A7) IN MODEL I

| IMFs | C1 | C2 | C3 | C4 | C5 | C6 | C7 |
|-------------------------|-------|-------|--------|-------|-------|--------|--------|
| Correlation coefficient | 1 | 4e-4 | -0.004 | 8e-4 | 0.008 | 0.037 | 0.894 |
| IMFs | C8 | C9 | C10 | C11 | C12 | C13 | r13 |
| Correlation coefficient | 0.933 | 0.292 | 0.008 | -3e-4 | -4e-5 | 1.5e-4 | 1.3e-4 |

TABLE V

THE CORRELATION COEFFICIENTS BETWEEN THE DETECTED SIGNAL AND ALL THE IMF'S RESPECTIVELY (THE SIGNAL IS IN THE CASE OF THE IMPULSE EMITTED FROM ANTENNA A5 AND RECEIVED BY ANTENNA A8) IN MODEL I

| IMFs | C1 | C2 | C3 | C4 | C5 | C6 | C7 |
|-------------------------|------|--------|--------|--------|--------|-------|-------|
| Correlation coefficient | 1 | -6.004 | -0.003 | -0.002 | -0.009 | 0.023 | 0.693 |
| IMFs | C8 | C9 | C10 | C11 | C12 | C13 | r13 |
| Correlation coefficient | 0.94 | 0.674 | -3e-4 | -0.001 | -2e-4 | 3e-6 | 9e-5 |

value is introduced in this paper to help the extraction of the tumor response more sensitively. The kurtosis value represents the degree of peakedness of a dataset and is represented as a ratio of the fourth central moment of the data to its squared variance. The kurtosis value is defined as follows [32], [33]:

$$kurt = \frac{E(c_n - \mu)^4}{(E(c_n - \mu)^2)^2} \quad (11)$$

where E is the expectation operator, the parameter μ represents the mean value of the n^{th} IMF, $E(c_n - \mu)^4$ is the fourth moment about the mean, and $E(c_n - \mu)^2$ is the standard deviation. The kurtosis of a Gaussian sequence is 3 [34]. In this way, the relations can be expressed in terms of the quantity: $Kurt = kurt - 3$, which is zero for the Gaussian distribution. The kurtosis is also commonly referred as gaussian unlikeliness, since a larger value of Kurt implies a stronger non-gaussianity. Kurtosis can be either positive or negative. Random variables that have a negative kurtosis are called sub-gaussian, and those with positive kurtosis are called super-gaussian. Super-gaussian random variables have typically a "spiky" probability density function. Sub-gaussian random variables, on the other hand, have typically a "flat" probability density function, which is rather constant near zero, and very small for values of the variable. The ultra-wide band (UWB) imaging technique for the breast cancer detection is developed intensively based on the contrast in the electric properties of malignant tumor related to normal fatty breast tissue [35]. The dielectric constant determines the ability of the material to store the electric field energy, while the loss factor indicates how much of that energy is converted into heat and dissipated. With a tumor present, waves traveling through the breast encounter a change in electrical properties, causing the incident wave to scatter. The scattering changes the amounts

TABLE VI

THE KURTOSIS VALUE OF ALL THE IMFs (THE SIGNAL IS IN THE CASE OF THE IMPULSE EMITTED FROM ANTENNA A1 AND RECEIVED BY ANTENNA A3) IN MODEL I

| IMFs | C1 | C2 | C3 | C4 | C5 | C6 | C7 |
|----------------|--------|-------|-------|-------|-------|-------|--------|
| Kurtosis value | 15.073 | 2.907 | 2.893 | 2.939 | 3.239 | 3.085 | 33.352 |
| IMFs | C8 | C9 | C10 | C11 | C12 | C13 | r13 |
| Kurtosis value | 14.066 | 6.381 | 6.192 | 5.314 | 3.639 | 1.789 | 2.040 |

TABLE VII

THE KURTOSIS VALUE OF ALL THE IMFs (THE SIGNAL IS IN THE CASE OF THE IMPULSE EMITTED FROM ANTENNA A3 AND RECEIVED BY ANTENNA A7) IN MODEL I

| IMFs | C1 | C2 | C3 | C4 | C5 | C6 | C7 |
|----------------|--------|-------|-------|-------|-------|-------|--------|
| Kurtosis value | 15.221 | 2.990 | 2.987 | 3.089 | 2.856 | 3.099 | 21.992 |
| IMFs | C8 | C9 | C10 | C11 | C12 | C13 | r13 |
| Kurtosis value | 12.978 | 8.268 | 4.672 | 3.741 | 2.364 | 1.621 | 2.605 |

TABLE VIII

THE KURTOSIS VALUE OF ALL THE IMFs (THE SIGNAL IS IN THE CASE OF THE IMPULSE EMITTED FROM ANTENNA A5 AND RECEIVED BY ANTENNA A8) IN MODEL I

| IMFs | C1 | C2 | C3 | C4 | C5 | C6 | C7 |
|----------------|-------|-------|-------|-------|-------|-------|--------|
| Kurtosis value | 8.526 | 2.968 | 3.071 | 2.915 | 2.793 | 3.000 | 29.023 |
| IMFs | C8 | C9 | C10 | C11 | C12 | C13 | r13 |
| Kurtosis value | 7.437 | 7.586 | 4.127 | 4.816 | 2.510 | 1.581 | 1.876 |

of energy detected at the receivers and the transmitter. The kurtosis is a descriptor originally devised to detect and to characterize transients in a signal. As the tumor has higher permittivity, the amounts of the scattered energy should be larger than the others. So the kurtosis value of the tumor signal should be higher than those of the other signals with clutters.

As shown in Tables VI–VIII, each of the 7th IMF (C7) obtained from the received signal has the largest kurtosis value among all the IMFs. It shows that the correlation coefficient of the 8th IMF (C8) is larger than the 7th IMF's. This can be understood that the 8th IMF (C8) is more correlated with the as-detected signal, so some clutters are still contained in the 8th IMF (C8). As the tumor has the largest dielectric constant, the signal of the tumor response should have the largest kurtosis value. This implies that 7th IMF (C7) contains most of the tumor response, which can be used to reconstruct the tumor image.

All the 7th IMFs that are obtained from all the received signals are processed by the confocal microwave imaging (CMI) approach [36], which is also called Delay-and-Sum, to form the image. The reconstructed image is created by time-shifting and summing data points from each integrated selected tumor signal (such as 7th IMF) for each synthetic focal point in the breast.

Authorized licensed use limited to: UNIVERSITY OF NEVADA RENO. Downloaded on October 09, 2023 at 05:39:25 UTC from IEEE Xplore. Restrictions apply.

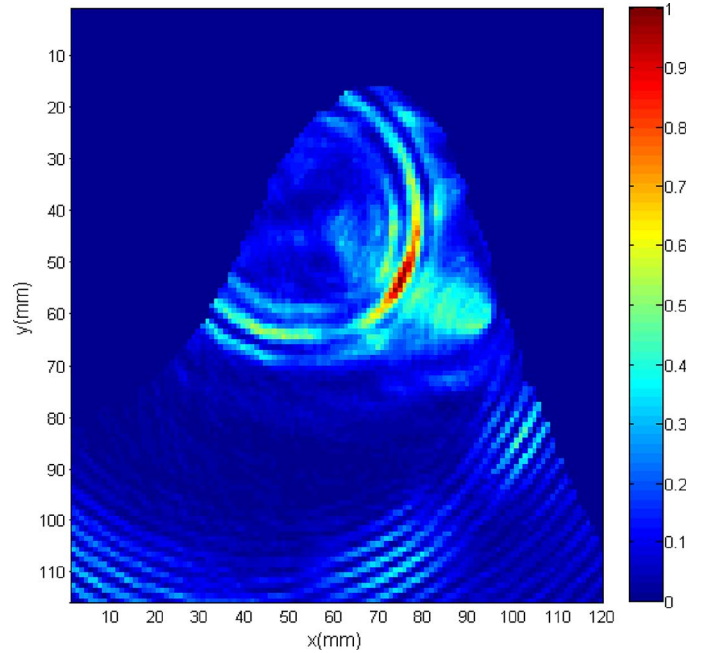


Fig. 9. Image reconstruction of Model I by employing the proposed optimal EEMD method.

The intensity of a pixel in the reconstructed image sum for a specific synthetic focal point is assigned to be the square of the coherently summed values

$$I(r) = \left[\sum_{i=1}^M (\psi_i \cdot X_i(r)) \right]^2 \quad (12)$$

where the weights ψ_i are introduced to compensate the radial spreading of each wave as it propagates from the transmitting antenna, and $X_i(r)$ is the time shifted signal. The results are shown in the next section.

IV. RESULTS AND DISCUSSION

A. Reconstructed Images of Model I

To test the proposed extraction method, a tumor with the diameter of 4 mm is inserted in the phantom shown in Fig. 2. In particular, the tumor is located within the glandular region. In the imaging process, the 7th IMFs (C7) of all the signals detected by the antenna array are applied in the CMI algorithm in our study. As presented in Fig. 9, the CMI algorithm is employed to create the reconstructed image of model I. This reconstructed image shows the correct tumor information. The correct position of the tumor can be observed clearly. This result verifies the correctness of the proposed extraction method in this study.

The tumor-free model is also used here for comparison to verify the accuracy of the result. Fig. 10 shows the result of using the calibration waveform that is obtained from the tumor-free model. By contrast, the result of using the proposed method

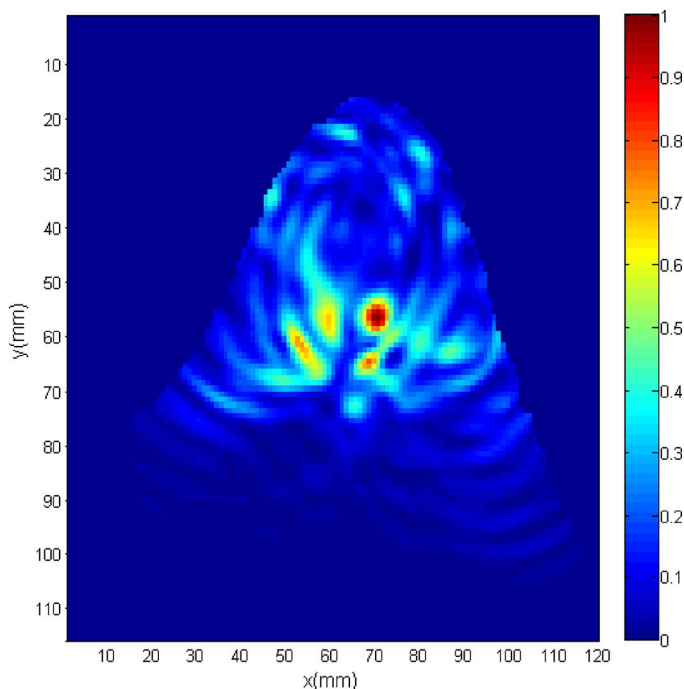


Fig. 10. Image reconstruction of Model I by employing tumor-free model for comparison.

in this paper is quite right compared to the previous work which uses the tumor-free model.

B. Reconstructed Images of Model II

The proposed approach is also tested for the case of higher noise level. For this purpose, model II shown in Fig. 4 is used. In this phantom, the dielectric constant contrast between the glandular and the tumor is very small. This allows the assessment of the detection system for the critical situation of reduced dielectric constant contrast between the tumor and the surrounding tissues. According to the same parameter selection procedure in model I, the parameters are set as $L = 2.0$ and $M = 50$ in model II. Fig. 11 shows the result of using the proposed method in this paper. The correct tumor information shown in the image verifies the correctness and the feasibility of our proposed method. It can be concluded that the result of using the proposed signal processing method in this paper gives the correct location of the tumor. For comparison, Fig. 12 gives the reconstructed image by adopting the tumor-free model.

In Figs. 9 and 11, the red color intensity represents tumor response as the red color represents the highest energy intensity. The tumor size and position can be recognized accurately, as shown in Fig. 9, the tumor is at the position of (71 mm, 55 mm). Also, as shown in Fig. 11, the tumor is at the position of (89 mm, 108 mm). They all have very small deviations from the exact tumor positions compared with the Model I shown in Fig. 2 and the Model II shown in Fig. 4. But these deviations are fine with the exact position shown in these two models.

The correctness of this tumor response extraction method can be verified from these four reconstructed images. It can be concluded that the tumor in the glandular region can also be distinguished successfully. The feasibility of this method is confirmed

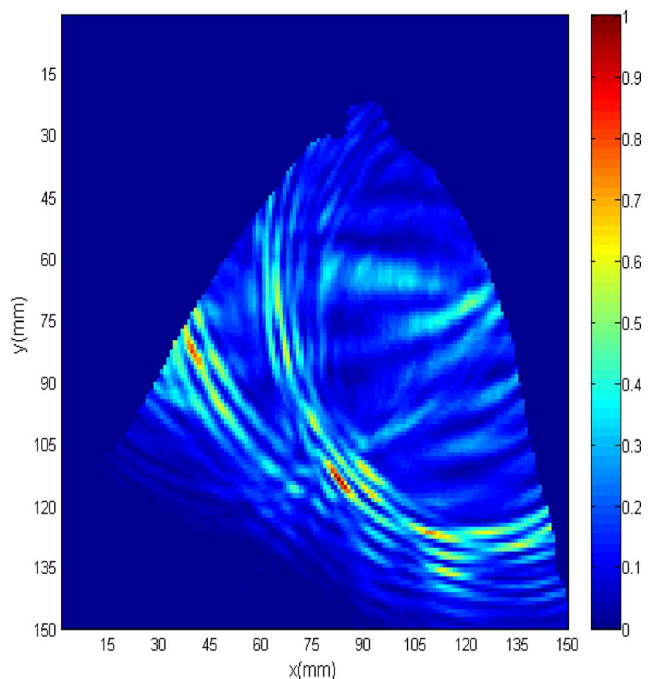


Fig. 11. Image reconstruction of Model II by employing the proposed optimal EEMD method.

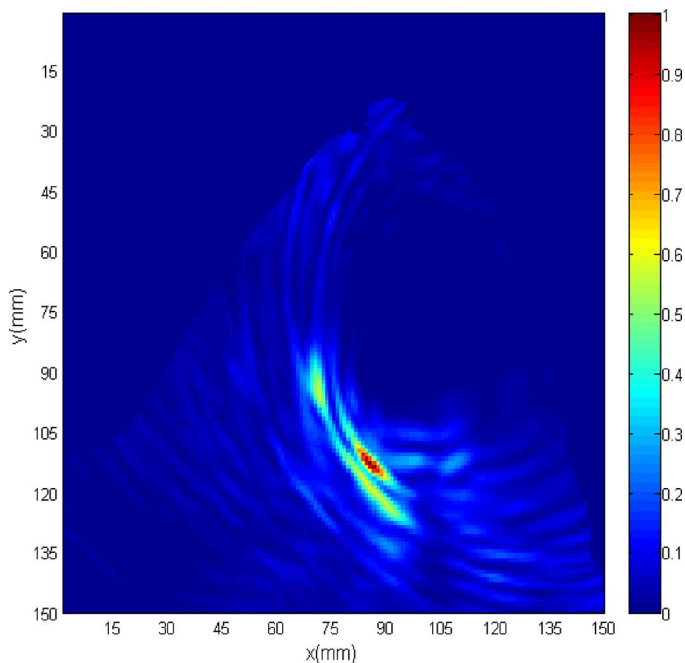


Fig. 12. Image reconstruction of Model II by employing tumor-free model for comparison.

by detecting a tumor with a diameter of 4 mm which is buried in the breast with a smaller dielectric constant contrast between the tumor and the glandular tissues. These results verify that this method could adapt to different types of the breast in clinical cases. This method could directly extract the tumor response from the as-detected signals. In this way, the detecting procedure can be much more efficient and convenient by using this method.

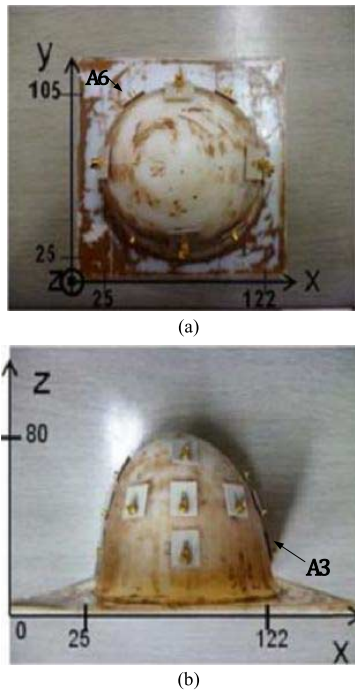


Fig. 13. Photograph of 3-D printed breast phantom with antennas attached on the surface. (a) Top view. (b) Side view.

C. Experiment Verification

The proposed approach is also tested by detecting a breast tumor phantom embedded in a 3-D printed breast model. The numerical data of the 3-D printed breast phantom was derived from the Class III numerical breast phantom in the University of Wisconsin Computational Laboratory (UWCEM) breast phantom repository [37].

The outer shell of the breast phantom is made of acrylonitrile butadiene styrene (ABS) plastic. The interior of this phantom is filled with Silicone and a solution of ethyl alcohol and water. The tumor phantom is made of a cured pork meat with the size of $10 \text{ mm} \times 10 \text{ mm} \times 10 \text{ mm}$, which is located at the bottom of the interior void at the position of $x = 55 \text{ mm}$, $y = 55 \text{ mm}$, $z = 30 \text{ mm}$. Fig. 13 shows the photograph of the breast phantom. The measurement set-up for breast cancer detection is shown in Fig. 14.

A radar-based breast cancer detection system was developed by using a wide-slot and a stacked patch antenna [38]. A compact 4×4 planar UWB antenna array with the total size of $44 \text{ mm} \times 52.4 \text{ mm}$ was developed for this system. The antenna used in this system consists of a square slot in a ground plane on one side of a Duroid RT 6010LM substrate with a relative permittivity of 10.2. A forked microstrip feed was formed on the other side. And this microstrip splits from a 50Ω feed into two 100Ω to excite the slot in the wide bandwidth [20]. The size of the slot antenna was $11.0 \text{ mm} \times 13.1 \text{ mm}$. SMP connectors were soldered. In this detecting system, the Agilent 81142A pulse pattern generator, E8361A oscilloscope, 34980A multifunction switch, MT-417 16 port RF switch box and SHF 810 power amplifier were also used to help this detection carry out. During this detection, there are 192 series of signals, which means 192 series of raw data, contributing in the imaging process.

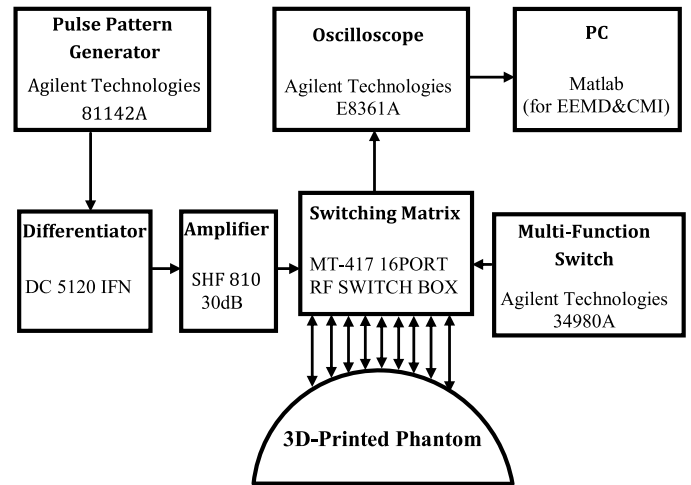


Fig. 14. Measurement set up for breast cancer detection.

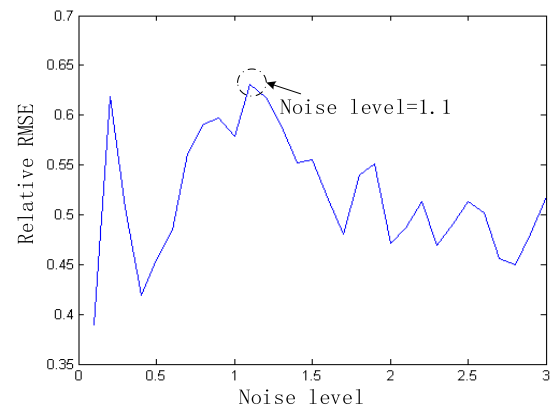


Fig. 15. The value of relative RMSE with different noise level for the experimental phantom.

In the detection system, a serial pulse data are firstly generated by the pulse pattern generator and transmitted to differentiator to form the Gaussian monocycle pulse (GMP) signal. Then the GMP is amplified by the amplifier and transmitted to the switching matrix. The switching matrix will guide the GMP signal to a certain transmitting antenna to illuminate the breast. A multi-function switch is used to control the switching matrix. Then the reflected signals are captured by the other antennas and chosen in turn by the switching matrix. Then the oscilloscope is used to read and record the reflected signals. After all the signals are recorded, the EEMD and CMI algorithms are used for signal processing and image reconstruction by a PC with MATLAB to find the position of the breast tumor.

After getting the as-detected signals, the proposed EEMD method is applied in extracting the tumor signal. In this detection, the noise level selection is shown in Fig. 15. It can be found that the noise level should be 1.1. And the ensemble number is 50, which is a proper number. The decomposition result of the detected signal in the case of the impulse emitted from antenna A6 and received from antenna A3 is shown in Fig. 16. After getting the decomposition results of all the as-detected signals, the correlation coefficients and the kurtosis values of all the IMFs are calculated. Table IX shows the correlation coefficients of all

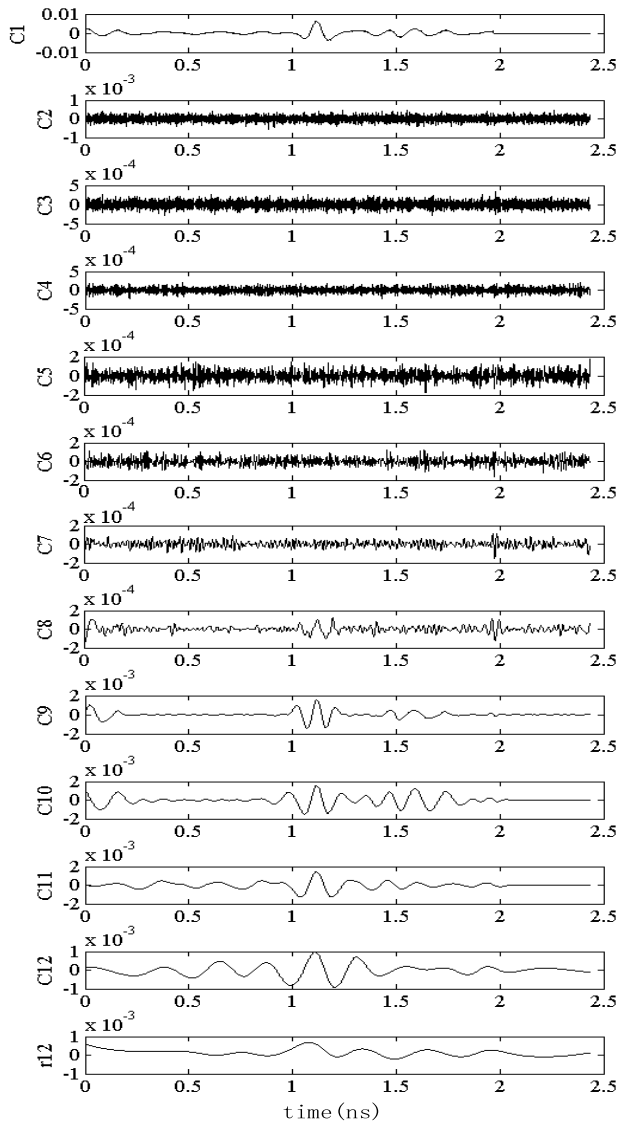


Fig. 16. IMFs (C1 to C13) of the detected signal for the experimental phantom in the case of the impulse emitted from antenna A6 and received from antenna A3. The r12 is the residual of the signal after the EEMD processing.

the IMFs obtained from the as-detected signal, which is in the case of the impulse emitted from the antenna A6 and received by the antenna A3. It can be found that the 9th IMF (C9), 10th IMF (C10), and 11th IMF (C11) have bigger correlation coefficients than the other IMFs. As shown in Table X, the 9th IMF (C9) obtained from the received signal has the biggest kurtosis value among these three IMFs (C9, C10, C11). In the case of the impulse emitted from antenna A6 and received from antenna A3, the 9th IMF (C9) is selected as the tumor responding signal. In this detection, the tumor signal is selected among the IMFs which have the bigger correlation coefficients. Then choose the IMF with biggest kurtosis value among the selected IMFs as the tumor signal. All the tumor signals extracted from all the as-detected signals are processed by the confocal microwave imaging (CMI) approach.

Figs. 17 and 18 show the results of using the proposed method in this paper. It can be found in these results that the tumor position is (50 mm, 50 mm, 30 mm), which has deviation with the

TABLE IX
THE CORRELATION COEFFICIENTS BETWEEN THE DETECTED SIGNAL AND ALL THE IMFs RESPECTIVELY (THE SIGNAL IS IN THE CASE OF THE IMPULSE EMITTED FROM ANTENNA A6 AND RECEIVED BY ANTENNA A3)

| IMFs | C1 | C2 | C3 | C4 | C5 | C6 | C7 |
|-------------------------|-------|--------|--------|-------|--------|-------|-------|
| Correlation coefficient | 1 | -0.003 | 1.5e-4 | -7e-4 | -0.008 | 0.011 | 0.013 |
| IMFs | C8 | C9 | C10 | C11 | C12 | r12 | |
| Correlation coefficient | 0.259 | 0.662 | 0.821 | 0.787 | 0.539 | 0.203 | |

TABLE X
THE KURTOSIS VALUE OF ALL THE IMFs (THE SIGNAL IS IN THE CASE OF THE IMPULSE EMITTED FROM ANTENNA A6 AND RECEIVED BY ANTENNA A3)

| IMFs | C1 | C2 | C3 | C4 | C5 | C6 | C7 |
|----------------|-------|--------|--------|--------|-------|--------|-------|
| Kurtosis value | 9.987 | 3.138 | 2.962 | 2.955 | 3.146 | 3.2555 | 4.049 |
| IMFs | C8 | C9 | C10 | C11 | C12 | r12 | |
| Kurtosis value | 5.179 | 9.9455 | 4.3862 | 6.4945 | 4.498 | 3.497 | |

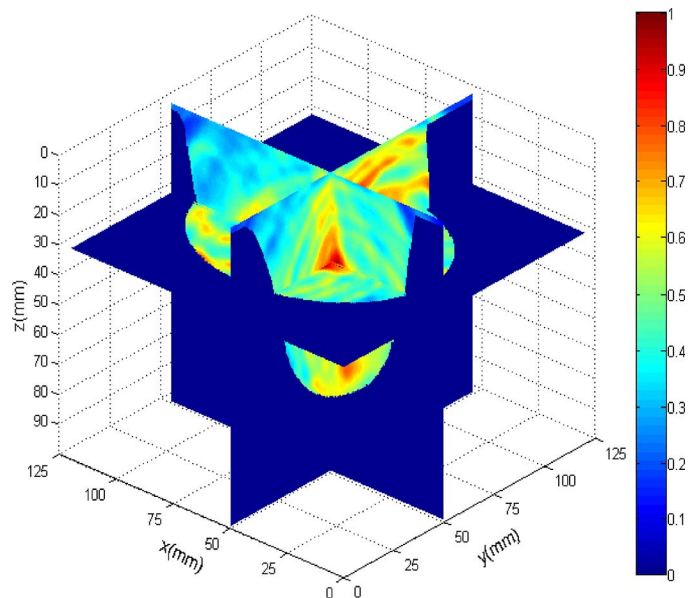


Fig. 17. Image reconstruction of the experimental phantom.

exact tumor position. The reason might be that the permittivity of the materials that are filled in the 3-D phantom and the permittivity of the outer shell of the breast phantom are different. The velocity of the microwave propagating in breast tissues is correlated with the permittivity of the materials. So the velocity of the signal will influence the accuracy of the results. It can be found in Figs. 9 and 11 that the detected locations of the tumors also have small deviations compared to the exact positions of the assumed tumors in the models. For model I, as shown in Fig. 2, the tumor is assumed at the position of (71 mm, 57 mm). The detection result with EEMD for model I is shown in Fig. 9, the tumor is located at (71 mm, 55 mm). Also, for model II shown in Fig. 4, the tumor is assumed at the position of (95 mm, 105 mm). The detection result with EEMD for model II is shown in Fig. 11, the tumor is located at (89 mm, 108 mm). For the experimental

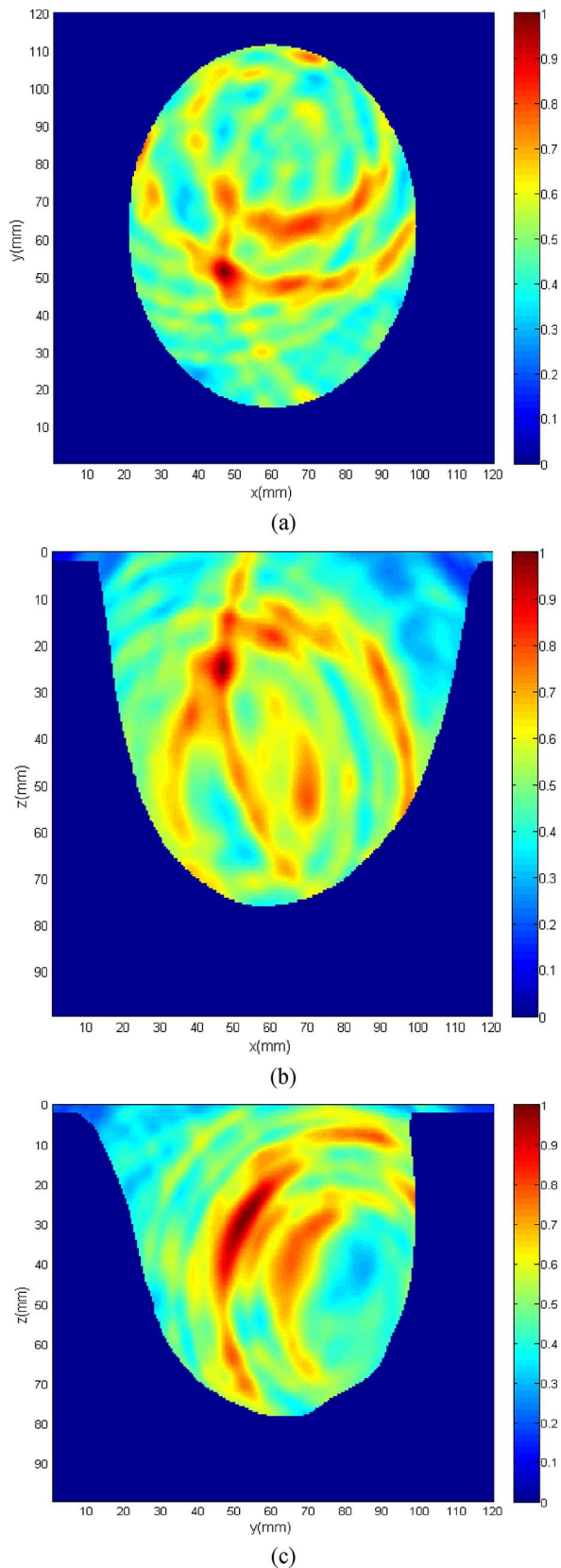


Fig. 18. Image reconstruction of the experimental phantom in slices (a) x-y plane, (b) z-x plane, and (c) z-y plane.

test, the tumor is inserted at the position of (55 mm, 55 mm, 30 mm). The detecting result with EEMD shown in the recon-

structed image is (50 mm, 50 mm, 30 mm). These deviations are acceptable with respect to the UWB breast tumor detection. The reason of the location deviation might be that the velocity of electromagnetic waves applied to the imaging process varies slightly due to the dielectric constant distribution in the complicated breast tissues. And some clutters from the interior of the breast still exist in the extracted tumor signal and the residue of the added white noise has not been cancelled completely. However, even using the subtraction method with the calibration waveform, which stands for the ideal situation, the results also have some deviations probably due to the value of the wave velocity used in the imaging algorithm. These limitations will be further investigated to improve our future study.

D. Comparison With Other Breast Cancer Detection Methods

Currently there are many other early breast cancer detection methods as shown in Table XI. The group of Hagness used distorted born iterative method (DBIM) for microwave breast imaging [39]. The group of Elise C. Fear developed a technique to estimate the internal structure of experimental objects using radar techniques [40]. The group of Maciej Klemm rotates the antenna array. Rotation gives them two sets of measured data, in which undesired signals such as antenna coupling, or skin reflections are almost identical and appear at the same time position, therefore they can be eliminated [41]. In [42], they use gold nanoparticles as the contrast agent to change the average electrical properties of cancerous tissues. The group of Carey M. Rappaport proposed a hybrid Digital Breast Tomosynthesis (DBT) and microwave Nearfield Radar Imaging (NRI) technique for detecting breast cancer [43]. The group of Takashi Takenaka proposed a three dimensional inverse scattering technique, called forward-backward time-stepping (FBTS), which is applied to the reconstruction of the microwave properties of the breast [44]. The group of P.M. Meaney proposed a clinical 3-D microwave tomographic imaging method for the breast, which is able to measure signals down to levels compatible with sub-centimeter image resolution and overcomes the enormous time burden [45]. And many other studies are extensively carrying out on the UWB breast cancer detection.

The proposed method in this paper is convenient in the sense that the components are derived directly from the data. The EEMD method is very adaptive, as its bases are amplitude/frequency modulated locally, data-adaptive, and sparse. This facilitates the discovery of intrinsic patterns at multiple scales, while not requiring the rigid assumptions of harmonic or stationary data structures. Also, the proposed method can directly extract the tumor signal from the as-detected signals. It is much more convenient than before as the tumor response extraction needs to subtract the calibration waveform in the past studies. The proposed method avoids using any calibration waveform. And it does not need complex equipment or large scale of calculation, which makes the detection process much more efficient and convenient in the future clinical application.

V. CONCLUSION

A tumor response extraction approach which can directly extract the tumor signal from the as-detected signals is presented in detail. The proposed method is based on the EEMD

TABLE XI
COMPARISON OF THE OTHER EARLY BREAST CANCER DETECTION METHODS

| Research Groups | Tumor signal extraction methods and early breast cancer detection methods | Strength & Limitations |
|----------------------------|---|--|
| Susan C.Hagness | The distorted born iterative method (DBIM) has been explored for microwave breast imaging [39]. | The proposed approach yields average property estimates that are close to the exact average and is an effective method for high-quality imaging with DBIM. Obtaining good results with DBIM requires patient specific estimates of the average properties. |
| Elise C.Fear | Developed a technique to estimate the internal structure of experimental objects using radar techniques [40]. | This effectively estimates the internal structure of the breast using radar techniques. The algorithm is capable of resolving features related to thin outer layers in a realistic scenario. |
| Maciej Klemm | 1. Rotate the antenna array [41]. 2. Add contrast agent (such as gold nanoparticles) [42]. | 1. Successfully detect 4 and 6 mm diameter spherical tumors in the curved breast phantom, but still needs the subtraction. 2. Nanoparticles could provide detectable changes in clinically relevant concentrations. |
| Carey M. Rappaport | A hybrid Digital Breast Tomosynthesis (DBT) and microwave Nearfield Radar Imaging (NRI) technique for detecting breast cancer [43]. | Successfully detect cancerous tissues in the breast, despite the low contrast that exists between the tumor and glandular tissue. The dielectric contrast between cancerous and normal glandular tissues in the breast is no more than about 10%. |
| Takashi Takenaka | Forward-backward time-stepping (FBTS) algorithm [44]. | Good detection of a 5 mm diameter tumor and discrimination of the various internal breast tissue types. But the computational complexity is big. |
| P.M. Meany | The clinical 3-D microwave tomographic images of the breast.[45] | First, the hardware is able to measure signals down to levels compatible with sub-centimeter image resolution while keeping an exam time under 2 min. Second, the software overcomes the enormous time burden and produces similarly accurate images in less than 20 min. |
| Previous work of our group | Shifting the whole linear antenna array during detection.[46] | The tumor of 5 mm in diameter can be detected by subtracting the signals obtained by the linear antenna array located at different places. However, this method still needs to subtract the calibration waveform, although it does not need to use the tumor-free model. |
| This Research | Proposed method of applying the EEMD algorithm in the signal processing | The proposed method offers the efficient detection for a tumor of 4 mm diameter. It is convenient, as it does not need to subtract any calibration signals. It does not need complex equipment or large scale of calculation. The results are with less accuracy than the exact location of the tumor. |

method. This method is applied in detecting two simulation models (Figs. 2 and 4) based on the clinical MRI images of two different patients, and one real prototype which is made by the

3D-printing based on the UWCEM breast phantom repository to simulate a real patient's breast shown in Fig. 13 [37]. Two different simulation models in which the different effects of the clutter of the glandular are taken into consideration during the imaging process to verify the feasibility of this proposed approach. Also, the experiment results confirm the correctness and the feasibility of the proposed method in this paper.

Consequently, the method given in this paper has the feasibility in detecting different cases of the breast with respect to the clinical cases. This proposed approach avoids the use of any calibration waveform of the tumor-free model. It has been shown that the proposed method offers the efficient detection even for a tumor of 4 mm diameter located within the glandular or at the interface between the gland and fat. The tumor response can also be extracted in the case that the glandular tissue has larger dielectric constant of 35. Our study indicates that the proposed approach can be an effective alternative to direct extraction of the tumor response.

ACKNOWLEDGMENT

The authors thank Z. Wang at Tianjin University for the configuration construction, discussion, and help.

REFERENCES

- [1] E. S. Hwang, D. Y. Lichtensztajn, S. L. Gomez, B. Fowble, and C. A. Clarke, "Survival after lumpectomy and mastectomy for early stage invasive breast cancer," *Cancer*, vol. 119, no. 7, pp. 1402–1411, 2013.
- [2] G. Eason, B. Noble, and I. N. Sneddon, "Artificial neural networks applied to cancer detection in a breast screening programme," *Math. Comput. Model.*, vol. 55, no. 12, pp. 983–991, 2008.
- [3] X. Xiao, L. Xu, and Q. W. Li, "A double constrained robust Capon beamforming based imaging method for early breast cancer detection," *Chin. Phys. B*, vol. 22, no. 9, p. 094101, 2013.
- [4] G. J. Bond, X. Li, S. C. Hagness, and B. D. Van Veen, "Microwave imaging via space-time beamforming for early detection of breast cancer," *IEEE Trans. Antennas Propag.*, vol. 51, no. 8, pp. 1690–1705, 2003.
- [5] X. Li, S. K. Davis, S. C. Hagness, D. W. van der Weide, and B. D. Van Veen, "Microwave imaging via space-time beamforming: Experimental investigation of tumor detection in multilayer breast phantoms," *IEEE Trans. Microw. Theory*, vol. 52, no. 8, pp. 1856–1865, 2004.
- [6] A. Basak, V. Ranganathan, and S. Bhunia, "Implantable ultrasonic imaging assembly for automated monitoring of internal organs," *IEEE Trans. Biomed. Circuits Syst.*, vol. 8, no. 6, pp. 881–890, 2014.
- [7] S. Brovoll, T. Berger, Y. Paichard, O. Aardal, T. S. Lande, and S. E. Hamran, "Time-lapse imaging of human heart motion with switched array UWB radar," *IEEE Trans. Biomed. Circuits Syst.*, vol. 8, no. 5, pp. 704–715, 2014.
- [8] M. Klemm, J. A. Leendertz, D. Gibbins, I. J. Graddock, A. Preece, and R. Benjamin, "Microwave radar-based breast cancer detection: Imaging in inhomogeneous breast phantoms," *IEEE Antennas Wireless Propag. Lett.*, vol. 8, pp. 1349–1352, 2009.
- [9] X. Xiao and T. Kikkawa, "Extraction of calibration waveform for confocal microwave imaging for early breast cancer detection," in *Proc. Int. Symp. Microw. Antenna Propagation and EMC Tech. for Wireless Commun.*, 2007, pp. 1287–1290.
- [10] X. Xiao and T. Kikkawa, "Influence of the organism interface on the breast cancer detection by UWB," *Appl. Surf. Sci.*, vol. 255, pp. 597–599, 2008.
- [11] Z. Zhao, L. Yang, D. Chen, and Y. Luo, "A human ECG identification system based on ensemble empirical mode decomposition," *Sensors*, vol. 13, no. 5, pp. 6832–6864, 2013.
- [12] M. Amarnath and I. R. Krishna, "Detection and diagnosis of surface wear failure in a spur geared system using EEMD based vibration signal analysis," *Tribol Int.*, vol. 61, pp. 224–234, 2013.
- [13] H. Jiang, C. Li, and H. Li, "An improved EEMD with multiwavelet packet for rotating machinery multi-fault diagnosis," *Mech. Syst. Signal Process.*, vol. 36, no. 2, pp. 225–239, 2013.

- [14] X. Chen, A. Liu, M. J. McKeown, H. Poizner, and Z. J. Wang, "An EEMD-IVA framework for concurrent multidimensional EEG and unidimensional kinematic data analysis," *IEEE Trans. Biomed. Eng.*, vol. 61, no. 7, pp. 2187–2198, 2014.
- [15] N. E. Huang and S. S. Shen, *Hilbert-Huang Transform and Its Applications*. Singapore: World Scientific, 2005, vol. 5.
- [16] J. Zhang, R. Yan, R. X. Gao, and Z. Feng, "Performance enhancement of ensemble empirical mode decomposition," *Mech. Syst. Signal Process.*, vol. 24, no. 7, pp. 2104–2123, 2010.
- [17] Y. Xie, B. Guo, L. Xu, J. Li, and P. Stoica, "Multistatic adaptive microwave imaging for early breast cancer detection," *IEEE Trans. Biomed. Eng.*, vol. 53, no. 8, pp. 1647–1656, 2006.
- [18] Z. J. Wang, X. Xiao, H. Song, L. Wang, and Q. W. Li, "Development of anatomically realistic numerical breast phantoms based on T1 and T2 weighted MRIs for microwave breast cancer detection," *IEEE Antennas Wireless Propag. Lett.*, vol. 13, pp. 1757–1760, 2014.
- [19] X. Xiao, H. Song, Z. J. Wang, and L. Wang, "A progressive processing method for breast cancer detection via UWB based on an MRI-derived model," *Chin. Phys. B*, vol. 7, no. 52, p. 074101, 2014.
- [20] T. Sugitani, S. Kubota, A. Toya, X. Xiao, and T. Kikkawa, "A compact 4×4 planar UWB antenna array for 3-D breast cancer detection," *IEEE Antennas Wireless Propag. Lett.*, vol. 12, pp. 733–736, 2013.
- [21] E. J. Bond, X. Li, S. C. Hagness, and B. D. Van Veen, "Microwave imaging via space-time beamforming for early detection of breast cancer," *IEEE Trans. Antennas Propag.*, vol. 51, no. 8, pp. 1690–1705, 2003.
- [22] M. Lazebnik, L. McCartney, D. Popovic, C. B. Watkins, M. J. Lindstrom, J. Harter, S. Sewall, A. Magliocco, J. H. Booske, M. Okoniewski, and S. C. Hagness, "A large-scale study of the ultra wide-band microwave dielectric properties of normal breast tissue obtained from reduction surgeries," *Phys. Med. Biol.*, vol. 52, pp. 2637–2656, 2007.
- [23] M. Lazebnik, D. Popovic, L. McCartney, C. B. Watkins, M. J. Lindstrom, J. Harter, S. Sewall, T. Ogilvie, A. Magliocco, T. M. Breslin, W. Temple, D. Mew, J. H. Booske, M. Okoniewski, and S. C. Hagness, "A large-scale study of the ultra wide-band microwave dielectric properties of normal, benign, and malignant breast tissues obtained from cancer surgeries," *Phys. Med. Biol.*, vol. 52, no. 20, pp. 6093–6115, 2007.
- [24] X. Chen, A. Liu, M. McKeown, H. Poizner, and Z. J. Wang, "An EEMD-IVA framework for concurrent multidimensional EEG and unidimensional kinematic data analysis," *IEEE Trans. Biomed. Eng.*, vol. 61, no. 7, pp. 2187–2198, 2014.
- [25] Z. Shen, N. Feng, Y. Shen, and C. H. Lee, "A ridge ensemble empirical mode decomposition approach to clutter rejection for ultrasound color flow imaging," *IEEE Trans. Biomed. Eng.*, vol. 60, no. 6, pp. 1477–1487, 2013.
- [26] Z. Wu and N. E. Huang, "Ensemble empirical mode decomposition: A noise-assisted data analysis method," *Adv. Adapt. Data Anal.*, vol. 1, no. 1, pp. 1–41, 2009.
- [27] K. T. Sweeney, S. F. McLoone, and T. E. Ward, "The use of ensemble empirical mode decomposition with canonical correlation analysis as a novel artifact removal technique," *IEEE Trans. Biomed. Eng.*, vol. 60, no. 1, pp. 97–105, 2013.
- [28] W. Guo and P. W. Tse, "A novel signal compression method based on optimal ensemble empirical mode decomposition for bearing vibration signals," *J. Sound. Vib.*, vol. 332, no. 2, pp. 423–441, 2013.
- [29] Q. W. Li, X. Xiao, H. Song, L. Wang, and T. Kikkawa, "Tumor response extraction based on ensemble empirical mode decomposition for early breast cancer detection by UWB," in *Proc. IEEE Biomedical Circuits and Systems Conf.*, 2014, pp. 97–100.
- [30] A. M. Neto, L. Rittner, N. Leite, D. E. Zampieri, R. Lotufo, and A. Mendeck, "Pearson's correlation coefficient for discarding redundant information in real time autonomous navigation system," in *Proc. IEEE Int. Conf. Control Applicat.*, 2007, pp. 426–431.
- [31] L. Schumacher and B. Raghoeaman, "Closed-form expressions for the correlation coefficient of directive antennas impinged by a multimodal truncated Laplacian PAS," *IEEE Trans. Wireless Commun.*, vol. 4, no. 4, pp. 1351–1359, 2005.
- [32] Z. L. Zhang and Z. Yi, "Extraction of a source signal whose kurtosis value lies in a specific range," *Neurocomput.*, vol. 69, no. 7, pp. 900–904, 2006.
- [33] V. Pakrashi, B. Basu, and A. O'Connor, "Structural damage detection and calibration using a wavelet-kurtosis technique," *Eng. Struct.*, vol. 29, no. 9, pp. 2097–2108, 2007.
- [34] R. Kuc, "Ultrasonic tissue characterization using kurtosis," *IEEE Trans. Ultrason., Ferroelectr., Freq. Control*, vol. 33, no. 3, pp. 273–279, 1986.
- [35] E. J. Bond, X. Li, S. C. Hagness, and B. D. Van Veen, "Microwave imaging via space-time beamforming for early detection of breast cancer," *IEEE Trans. Antennas Propag.*, vol. 51, no. 8, pp. 1690–1705, 2003.
- [36] X. Li and S. C. Hagness, "A confocal microwave imaging algorithm for breast cancer detection," *IEEE Microw. Wireless Compon. Lett.*, vol. 11, no. 3, pp. 130–132, 2001.
- [37] UWCEM Breast Phantom Repository [Online]. Available: <http://uwcem.ece.wisc.edu>
- [38] D. Gibbins, M. Klemm, I. J. Craddock, J. A. Leendertz, A. Preece, and R. Benjamin, "A comparison of a wide-slot and a stacked patch antenna for the purpose of breast cancer detection," *IEEE Trans. Antennas Propag.*, vol. 58, no. 3, pp. 665–674, 2010.
- [39] F. Gao, B. D. Van Veen, and S. C. Hagness, "Sensitivity of the distorted born iterative method to the initial guess in microwave breast imaging," *IEEE Trans. Antennas Propag.*, vol. 63, no. 8, pp. 3540–3547, 2015.
- [40] D. Kurrant and E. C. Fear, "Defining regions of interest for microwave imaging using near-field reflection data," *IEEE Trans. Microw. Theory Tech.*, vol. 61, no. 5, pp. 2137–2145, 2013.
- [41] M. Klemm, I. J. Craddock, J. A. Leendertz, A. Preece, and R. Benjamin, "Radar-based breast cancer detection using a hemispherical antenna array-experimental results," *IEEE Trans. Antennas Propag.*, vol. 57, no. 6, pp. 1692–1704, 2009.
- [42] M. Klemm, I. J. Craddock, and A. Preece, "Contrast-enhanced breast cancer detection using dynamic microwave imaging," in *Proc. IEEE Antennas and Propagation Soc. Int. Symp.*, 2012, pp. 1–2.
- [43] J. A. Martinez Lorenzo, R. Obermeier, F. Quivira, C. M. Rappaport, R. Moore, and D. B. Kopans, "Fusing digital-breast-tomosynthesis and nearfield-radar-imaging information for a breast cancer detection algorithm," in *Proc. IEEE Antennas and Propagation Soc. Int. Symp.*, 2013, pp. 2038–2039.
- [44] J. E. Johnson, T. Takenaka, K. A. H. Ping, S. Honda, and T. Tanaka, "Advances in the 3-D forward-backward time-stepping (FBTS) inverse scattering technique for breast cancer detection," *IEEE Trans. Biomed. Eng.*, vol. 56, no. 9, pp. 2232–2243, 2009.
- [45] T. M. Grzegorzczak, P. M. Meaney, P. A. Kaufman, R. M. di-Florio-Alexander, and K. D. Paulsen, "Fast 3-D tomographic microwave imaging for breast cancer detection," *IEEE Trans. Med. Imag.*, vol. 31, no. 8, pp. 1584–1592, 2012.
- [46] X. Xiao, Q. W. Li, L. Xu, H. Song, and L. Wang, "UWB imaging: Aids breast cancer," *Microw. RF*, vol. 53, no. 5, pp. 99–103, 2014.



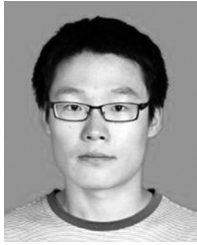
Qinwei Li received the B.S. and M.S. degrees in electronic science and technology from Tianjin University, Tianjin, China, in 2012 and 2015, respectively.

Currently, she is working toward the Ph.D. degree in electronic science and technology at Tianjin University. Her research interests include imaging algorithm, medical imaging, and signal processing.



Xia Xiao (M'01) received the B.S. degree in physics and the M.S. degree in condensed physics from Tianjin Normal University, Tianjin, China, in 1993 and 1996, respectively, and the Ph.D. degree in electronic and information technology from the Technical University of Chemnitz (TU Chemnitz), Chemnitz, Germany, in 2002.

From 2002–2003, she contributed to the "MIRAI Project" at the National Institute of Industrial Science and Technology (AIST), Tokyo, Japan, where she worked in ULSI low-k/Cu interconnect technology as a Key Researcher. In 2003, she joined the School of Electronic Information Engineering, Tianjin University, Tianjin, China, where she is currently a Professor. From 2006–2007, she was a Visiting Professor at Hiroshima University, Hiroshima, Japan, where she worked in developing algorithms for UWB imaging for early breast cancer detection. Her research interests include advanced algorithms for early breast cancer detection by UWB and non-destructive characterization of film properties by surface acoustic waves (SAWs).



Liang Wang received the B.S. and M.S. degrees in electrical information engineering from Tianjin University, Tianjin, China, in 2010 and 2013, respectively.

Currently, he is working toward the Ph.D. degree in electrical information engineering at Tianjin University. His research interests include medical imaging and numerical method in biomedical engineering, including microwave breast cancer detection as well as signal processing in interdisciplinary problems.



Hang Song received the B.S. and M. S. degrees in electronic science and technology from Tianjin University, Tianjin, China, in 2012 and 2015, respectively.

Currently, he is working toward the Ph.D. degree at Hiroshima University, Hiroshima, Japan. His research interests are microwave breast cancer detection system, complex permittivities of breast cancer tissues, and antenna design.



Hayato Kono received the B.S. degree in electrical engineering from Hiroshima University, Hiroshima, Japan, in 2014.

Currently, he is working toward the M.S. degree in the Graduate School of Advanced Sciences of Matter at Hiroshima University, Hiroshima, Japan. His research interest is breast cancer detection.

Peifang Liu received the M.D. degree from the Medical Faculty of the University of Zurich, Zurich, Switzerland.

She has been working in the Department of Diagnostic Radiology (Breast Imaging), Cancer Hospital of Tianjin Medical University, Tianjin, China. As a Resident Doctor, Attending Doctor, Associate Chief-Doctor, and Chief-Doctor in the Department of Radiology, Cancer Hospital of Tianjin Medical University, she has mainly engaged in conventional general radiological diagnosis, mammography, CT, and MR diagnosis, and now focuses on MR and breast imaging.

Hong Lu received the M.D. degree from Tianjin Medical University, Tianjin, China.

She has been working in the Department of Diagnostic Radiology, Cancer Hospital of Tianjin Medical University, Tianjin, China. As a Resident Doctor, Attending Doctor, and Associate Chief-Doctor in the Department of Radiology, Cancer Hospital of Tianjin Medical University, she has mainly engaged in conventional general radiological diagnosis, CT, and MR diagnosis, and now focuses on MR imaging.



Takamaro Kikkawa (S'74–M'76–SM'01–F'10) received the B.S. and M.S. degrees in electronic engineering from Shizuoka University, Shizuoka, Japan, in 1974 and 1976, respectively, and the Ph.D. degree in electronic system from the Tokyo Institute of Technology, Tokyo, Japan, in 1994.

In 1976, he joined the NEC Corporation, Tokyo, Japan, where he conducted research and development on interconnect technologies for large scale integrated circuits and dynamic random access memories. From 1983 to 1984, he was the Visiting Scientist at the Massachusetts Institute of Technology, Cambridge, MA, USA, where he conducted research on SOI transistors. In 1998, he joined the faculty of Hiroshima University, Hiroshima, Japan, where he is Professor of the Graduate School of Advanced Sciences of Matter and Director of the Research Institute for Nanodevice and Bio Systems. He is also Councilor of Hiroshima University. From 2001 to 2008, he was appointed the Senior Research Scientist at the National Institute of Advanced Industrial Science and Technology, Tsukuba, Japan, and the Group Leader of Low-k/Cu Interconnect Technology of Japan's "MIRAI Project." His research interests include wireless and wired interconnect technologies, impulse-radio-CMOS transceiver circuits with on-chip antennas, and impulse-radar-based CMOS breast cancer detection systems.

Dr. Kikkawa is a Fellow of Japan Society of Applied Physics.